LRP 359/88 November 1988

NON LINEAR RESPONSE OF PLASMA IONS IN LINEAR ELECTROSTATIC WAVES

F. Anderegg, F. Skiff, P.J. Paris, T.N. Good
M.Q. Tran, N. Rynn and R. Stern

Invited Paper presented by

F. Anderegg

at the

International Workshop "Nonlinear Phenomena in Vlasov Plasmas"
July 11-16, 1988
Cargèse, (Corsica,France)

NON LINEAR RESPONSE OF PLASMA IONS IN LINEAR ELECTROSTATIC WAVES

F. Anderegg , F. Skiff , P.J. Paris , T.N. Good
M.Q. Tran , N. Rynn* and R. Stern +

Centre de Recherches en Physique des Plasmas
Association Euratom - Confédération Suisse
Ecole Polytechnique Fédérale de Lausanne
21, Av. des Bains CH - 1007 Lausanne / SWITZERLAND

* University of California at Irvine, CA92717
+ University of Colorado, Boulder, CO80309

ABSTRACT

We present experiments which test the applicability of the Hamiltonian single particle theory to wave-particle interactions. This theory describes the chaotic acceleration of plasmas ions by electrostatic waves. The Hamiltonian description gives predictions about the threshold, fast time scale, details of the distribution function and conservation of three integrals of the motion while some of the integrals have been broken by the overlap of resonances.

Both electrostatic ion cyclotron and Bernstein waves are launched from antennae at the plasma boundary. Ion motions are observed by Laser Induced Fluorecence (LIF) and optical tagging.The linear response of the ion to the wave is distinguished from the chaotic response.

Several predictions of the single particle theory are observed in the experiments. In addition, evidence of self-consistent effects have been observed.

INTRODUCTION

The interaction between waves and charged particles is of fundamental importance in plasma physics. Here we will consider the particular case of ions interacting with electrostatic waves in a magnetic field. That magnetized ions may become stochastic with the application a of single propagating electrostatic wave has been shown theoretically. Stochastic motion results when particles are in a region of phase space where the trapping regions of at least two resonances are wide enough (considered separately) that they overlap[1-4].

Stochasticity has been proposed as an explanation for tokamak ion heating in the presence of lower hybrid waves[3,5], ion Bernstein waves[6] and drift Alfven waves[7]. Stochasticity has also been proposed as an ion heating mechanism in the magnetosphere[8]. The experimental observation of stochastic electron heating in a standing plasma wave has been reported by Doveil[9]. We have observed stochastic ion heating due to neutralized ion Bernstein waves[10].

In this paper, Vlasov theory of a hot plasma is used to describe linear waves in a magnetized plasma. The particle response consists of a linear part (the dielectric response) and of non-linear effects such as intrinsic stochasticity. By intrinsic stochasticity we mean the apparently chaotic trajectories of particles subject to purely deterministic forces. The interaction between a single charged particle and an electrostatic wave is described by a Hamiltonian. Classical Hamiltonian stochasticity has a recognized importance in the study of many systems[11]. Under certain circumstances intrinsic stochasticity may resemble a classical stochastic process[12]. In plasma wave-particle interactions, phase decorrelation between a particle and a wave frequently results in similar particle energy gains in the plasma frame, whether the decorrelation is brought about by intrinsic or extrinsic (e.g. collisional) process. Heating due to intrinsic stochasticity can be distinguised by a threshold , by a fast time scale and by details in the particle distribution function . In addition, a Hamiltonian description of wave particle interaction generally contains symmetries (conservation laws) which would not be present for a competing classically stochastic process. These symmetries imply restrictions on the transport, in phase space, of chaotic trajectories[13].

This paper reports the results of experiments, in both an argon plasma and a barium Q-machine plasma, where the conditions necessary for stochastic ion motion are created by externally excited electrostatic ion cyclotron waves and neutralized ion Bernstein waves. Both the linear and non-linear response of the plasma ions is detected using laser induced fluorescence (LIF) and optical tagging. In addition to electric probes, the linear dielectric response provides information on the waves[14,15].

In several respects the experimental results agree with single particle theory. However, they indicate also the presence of self consistent effects due to the modification of the particle distribution function by the waves.

EXPERIMENTAL SET-UP AND LIF DIAGNOSTIC

Experimental observations of wave particle interactions are performed in the LMP device[16] using argon gas discharge plasma or barium Q-plasma. In both cases the plasma can be up to 475 cm long and 5 cm in diameter in a uniform magnetic field $B \leq 0.3$ T ($\Delta B / B \leq 0.3$ %) . In the discharge (respectively Q-plasma) temperature of $T_e \sim 10$ eV and $T_i \sim 0.4$ eV ($T_e \sim T_i \sim 0.15$ eV) and densities of $n_e \sim 10^{11}$ cm^{-3} ($n_e \sim 10^9$ cm^{-3}) are typical. Low density barium Q-plasmas are ideal for studies of collisionless plasma physics being suitable for laser induced fluorescence (LIF) and optical tagging.

The Laser Induced Fluorescence (LIF) technique is based on laser excitation of transitions between quantum states of ions (or neutral atoms) in a plasma[17]. This method is able to measure ion densities, velocities (Doppler shift), temperatures (Doppler broadening), electron temperature (density of states), and magnetic fields (Zeeman splitting). Indirectly, even weak electric fields can be measured[14,18].

A variant of LIF is optical tagging [19]. A long lived metastable state is selectively populated by laser excitation of an ionic transition. This population is created in the volume defined by the intersection of the laser beam with the plasma. Having the same mass and charge as other ions, the metastable ions may be used as test particles. A search laser is used to detect the appearance of test particles at various positions in the plasma volume. In

addition to positional information, tagging can also determine the velocity-space motion of a particular group of ions with a given initial velocity.

Figure 1a shows the ionic transitions used in argon plasma. Since all the transitions starting from the ground state are in the deep UV, where no tunable lasers are available, we work with the population of the ArII $3d^2G_{9/2}$ metastable state which is populated by electronic collisions . This level represents few percent of the ion population. In the case of BaII (figure 1b) the ground state is the $6^2S_{1/2}$ level which is connected to other levels by two visible transitions. The two 5^2D states are long lifetime metastable states ($\tau \approx 1$ S) ,which live longer than the ion confinement time in the machine (≈ 4mS) .

The experimental set up for optical tagging is shown in figure 2. The tag beam is a pulsed laser (10 nS) in order to have a good temporal resolution.

ELECTROSTATIC WAVES

Since we are interested in wave particle interaction, a brief introduction to the electrostatic waves involved are presented in this section.

The dispersion relation for electrostatic waves in a magnetized hot plasma has principally two roots in the ion cyclotron frequency range[20]. The electrostatic ion cyclotron (acoustic) wave :

$$\omega^2 \approx \left(k_z^2 + \frac{\omega^2}{\omega^2 - \Omega_{ci}^2} k_\perp^2 \right) C_s^2 \quad \text{with } C_s^2 = \frac{2KT_e}{m_i} \qquad (1)$$

and the ion Bernstein wave :

$$\sum_{n=1}^{\infty} I_n(\Lambda_i) \frac{n^2}{(\omega/\Omega_{ci})^2 - n^2} \approx 0 \qquad \text{with } \Lambda_i = \left(\frac{k_\perp v_{thi}}{\Omega_{ci}} \right)^2 \qquad (2)$$

I_n is the modified Bessel function of order n. The dispersion relation is shown in figure 3 along with data from an argon gas discharge with B = 2kG . Solid curves represent the dispersion relation, and dashed curves indicate the level of linear damping. The waves are launched by a series of plates at the plasma edge which couple capacitively to the plasma column [21]. The parallel wavelength is determined by the size and separation of the plates along the magnetic field.

In the case of a barium Q-plasma the situation is complicated by two effects. The window in ω/k_z where undamped waves can be excited is more narrow due to the fact that $T_e \approx T_i$. Secondly, the plasma has a fast parallel drift introducing a large Doppler shift in the laboratory frame. The second harmonic branch of the dispersion relation is shown in figure 4a. The continuous line indicates the EICW and the dotted line the NIBW. The dashed lines indicate the damping. Figure 4b extends over a wider frequency range. Triangles are the experimental data and the theory is given by continnous lines.

Since our experiments involve a threshold in the electric field of the wave, a nonperturbative technique for measuring the amplitude of the wave electric field is essential. We measure wave amplitude through the linear dielectric response of the ions[14]. This response contains information on the perpendicular electric field and wave number. More details on this technique will be presented in a contributed paper of this workshop[15].

HAMILTONIAN SYSTEM

In order to describe the wave particle interaction, we use a simple model which consists of a single charged particle in a homogeneous magnetic field interacting with a propagating electrostatic wave. This situation can be conveniently described by a Hamiltonian.

Smith and Kaufmann[1] and Karney and Bers[3] have shown numerically that in such a system intrinsic stochasticity may arise.

We are considering a cylindrical wave and therefore we use the pairs of canonicaly conjugate variables (z,p_z), (ϕ,p_ϕ) and $(\theta,1/2m\Omega R^2)$. Where z is the direction along the magnetic field, ϕ is the angular position of the particles around the guiding center and θ and R are the cylindrical coordinates of the guiding center. We will assume that the magnetic field $\underline{B}$ is along the z direction.

In the reference frame moving along the magnetic field with the wave we have :

$$H = \frac{p_z^2}{2m} + p_\phi \Omega_{ci} + e\,\Phi_0 \sin\left(k_z z + k_\perp R - k_\perp \rho_i \sin(\phi + \theta)\right) \qquad (3)$$

with $\rho_i = \left(\frac{2p\phi}{m\Omega_{ci}}\right)^{\frac{1}{2}}$ being the particle gyroradius and Φ_0 is the wave potential.

Although the particle energy is conserved in the wave frame, the onset of stochasticity usually results in a change in particle energy in the laboratory frame.

The Hamilton's equations are derived from the above Hamiltonian. Time is normalized to the ion cyclotron frequency Ω_{ci} ,length to parallel wave number k_z and impulsion to $k_z/m\Omega_{ci}$. Numerical time integration of the Hamilton equations is performed. A Poincaré section is taken by sampling the particle position each time the particle has completed a revolution around the field lines ($\phi = n\,2\pi$) .

Figures 5 and 6 present respectively a Poincaré section plot for 64 particles in the p_z-z plane and p_z-ρ plane for different values of the stochasticity parameter :

$$\varepsilon = \frac{k_z^2\, e\, \Phi_0}{m\, \Omega_{ci}^2} \qquad (4)$$

In the plane p_z-ρ the initial conditions are close to the experimental conditions. In the first graph ($\varepsilon = 0.0314$) particles remain close to their initial conditions.

In order to have a more complete picture of particle evolution in the p_z-z plane, particles have been initially distributed along the p_z axis .

All phase space plots represent the evolution of the particle trajectory during a time of 4000 Ω_{ci}^{-1} .

Since the Hamiltonian in the wave frame is a constant for each particle, the quality of the numerical integration can be checked to identify numerical noise in the particle trajectories. $\Delta H / H$ has been kept below 10^{-7}.

Figure 6c indicates the presence of particle acceleration in the laboratory frame if ε is above threshold. The experiments also indicate particle acceleration. Figure 7a and 7b are perpendicular and parallel ion distribution functions for a wave amplitude which exceeds the threshold value in barium plasma.

Figure 8 indicates experimental evidence of a threshold in the dependence of ion temperature on rf antenna current. Observation of the dielectric

response[14,15] allows an absolute measurement of the wave potential Φ_0 and the wave vector which are used to determine the experimental value of the wave stochasticity parameter.

The numerical and the experimental threshold are in good agreement for ion Bernstein wave. This comparison has to be made with the threshold given by Karney[3] for perpendicular propagation :

$$c\frac{E_\perp}{B_0} \approx \frac{1}{4}\left(\frac{\Omega_{ci}}{\omega}\right)^{\frac{1}{3}} \cdot \frac{\omega}{k_\perp} = 1.3 \times 10^4 \text{ [cm/sec]} \qquad (5)$$

Experimentally, $c\frac{E_\perp}{B_0} \approx 3 \times 10^4$ [cm/sec] as measured through the dielectric response

Above the threshold, broadening of the distribution function occurs very quickly as indicated in figure 9. The heating is clearly much faster than any ion collision time and therefore cannot be attributed to a collisional mechanism.

By taking measurements synchronously with the wave, we can insure that the particle acceleration (broadening of the distribution function) is not due to the linear response of the ions to the wave field (coherent oscillation of the distribution function at the wave frequency) .

CONSERVATION LAWS

The above Hamiltonian *(Eq. 3)* contains symmetries. Immediately it can be seen that H itself is a constant of motion because

$$\frac{\partial H}{\partial t} = 0 \qquad (6)$$

This implies, as mentioned above, that particle energy is a constant of motion in the wave frame. In other words, H has a translational invariance in time. In addition, the Hamiltonian is translationally invariant in the two directions perpendicular to the wave vector $\underline{k}$. This invariance results in conservation of the momenta p_θ and p_η , where $\underline{\eta} = \underline{k}\times\underline{k}\times\underline{B}$. In a magnetic field $\underline{B}$=(O,O, B_O) we have :

$$p_\theta = 1/2\, m\, \Omega\, (R^2 - \rho^2) \qquad = C_1 \qquad (7)$$

$$p_\eta = \frac{k_{||} m \Omega R \theta - k_\perp p_z}{|k|} \approx C_2 \qquad (8)$$

(8) is strictly valid only in the limit $R^2 \gg \rho^2$

The contants C_1 and C_2 depend on the particle initial conditions. If the Larmor radius is small compared to the guiding center coordinate R, then R is nearly constant during the motion i.e. the particle guiding center will not move along the direction defined by $k_\perp$.

The conservation law $p_\eta = C_2$ is valid provided that $R^2 \gg \rho^2$. Conservation of p_η implies a displacement which is linked to acceleration along the magnetic field.

Each of the three conservation laws of the wave particle Hamiltonian has the effect of constraining the phase-space excursion of particles even during stochastic motion.

We will be considering particles which are several gyroradii away from the axis which, therefore, satisfy the above relation. Integration of the dynamical equations which follow from the Hamiltonian *(Eq. 3)* indicates the conservation laws clearly. Figures 6, 10 and 11 show results from this integration. The three pairs of frames are Poincaré section plots demonstrating the behaviour of particle orbits both below [6a,10a,11a] and above [6c, 10b, 11b] the threshold for stochastic motion. Below threshold, subsequent intersections of particle orbits with the plane of section are very close to the initial conditions and indicate regular motion.

Conservation of H during stochastic motion is illustrated in Fig. 6c The arc $1/2m\, p_z^2 + 1/2\, m\Omega^2\rho^2$ corresponds to the particle kinetic energy in the wave frame. A finite width is observed to this arc because of the contribution of the potential energy of the wave. An important consequence of the conservation of H is that, in the lab frame, stochasticity will change p_z primarily in the direction of wave travel provided that the particle initial perpendicular velocity is less than the wave parallel phase velocity. In the velocity plane, particle motion is restricted to lie on arcs centered on the wave parallel phase velocity. Experiment does indicate an asymmetry in the particle acceleration in the direction of propagation of the wave (-z) (figure 7b).

Furthermore, particle acceleration along arcs in velocity space centered on the wave parallel phase velocity ($\approx 1.8 \cdot 10^5$ cm/sec) is consistent with the range of energies observed ($\varepsilon < 4.5$ eV).

In figure 10 a series of particles have been started along a vertical chord (in real space) which is normal to B. This is done for the purpose of comparison with the experiment. The circle indicates the symmetry axis of the wave fields and the plasma size. For a group of particles with the initial conditions shown in figure 10a, conservation of p_θ results in the formation of a ring in physical space (figure 10b). R is nearly constant for off axis particles. If the wave-particle interaction causes ρ to increase (figure 6c) R will increase slightly. Experimentally, optical tagging provides a way of following ions in phase space . For these experiments, a pulse laser is used to quickly (≈10nsec) create metastable particles along a vertical chord at a given axial position, and a cw laser beam on a movable carriage[22] is used to detect test particles as a function of position, time, and velocity (figure 2). Figure 12 shows the results from such a scan both below and above the stochasticity threshold. Below threshold, particles move along the straight field lines. The large-dash curve in figure 12 is the plasma electron density profile. Short dashes are used on the same figure to indicate the excess metastable density profile at a distance of 27 cm (sensitivity x10) produced by the pump laser in the presence of a wave below the threshold. At a wave amplitude which exceeds the threshold for parallel accelarations, metastable particles are also found at the symmetric point about the wave axis on the horizontal chord. Thus, we infer that the test particles are forming a ring in configuration space which intersects the horizontal scan in two places. This ring formation is what one would expect (figure 10b) from the conservation of p_θ .

The link between guiding center motion in the $\underline{k} \times \underline{B} = \underline{\theta}$ direction and parallel acceleration implied by conservation of p_η is shown in figure 11b. Note that in figure 11 we plot the particle position (ψ, r) which differs slightly from the guiding center position (θ, R), but is what we measure experimentally. Experimentally, this correlation is most easily seen through changes in the time of flight of test particles as they move between the pump and search laser beams. Although the motion is chaotic, the parallel velocity

is not unbounded and, given the net Δp_z for a particle, the change in time of flight can be approximated by:

$$\Delta t \sim \Delta z v_D - \Delta z/(v_D + 1/2\Delta p_Z/m) \qquad (9)$$

where V_D is the nominal parallel drift of the Q-plasma. Using $\Delta\theta=\pi$ and *(Eq. 8)* one obtains $\Delta t \approx 20$ μsec. Figure 13 shows two time-of-flight spectra at diametrically opposed points on the horizontal chord. Those which remain at $\Psi\approx 0$ have a longer time of flight, on the average, than those which have been transported to $\Psi\approx\pi$. The peaks of these spectra are separated by the 20 μsec predicted above.

The three measurements presented above argue for the conservation of H, p_θ and p_η respectively. Despite the broadening of the distribution function which results from exceeding the stochasticity threshold, the individual particle motions continue to observe the basic symmetries of the wave-particle interaction Hamiltonian. Chaos during wave-particle interaction is seen to produce rapid, though constrained, transport of particles in coordinate space as well as in velocity space.

SELF-CONSISTENT EFFECTS

The linear wave theory gives a satisfying description even when the particle distribution is strongly modified by stochastic particle acceleration. Nevertheless three evidences of self-consistent effects are observed.

Because the wave vector, particulary of the NIBW, is sensitive to ion temperature, the perpendicular wavelength is observed to change (increase) with increased ion temperature. Therefore the threshold increases with ion temperature which may tend to saturate the process as observed in figure 9. Wave coupling may also change with the ion distribution function.

Another complication occurs when the parallel distribution is broadened. Given the heated distribution (figure 7b), the waves should continue to be strongly (linear Landau) damped even after they have decayed to a level below the threshold.

Figure 14a shows the temporal ion temperature evolution after the electrostatic wave has been excited above threshold. Figure 14b presents the in-phase component of the dielectric response indicating that the observed

ion temperature transient effects are associated with wave amplitude oscillations.

CONCLUSION

Several points of agreement exist, therefore between these experiments and the predictions of the single particle stochasticity theory. The threshold, the time required, the form of the distribution function, the conservation of three constants of motion all seem to agree with single particle theory.

The linear wave theory appears to hold throughout. Despite the self consistent effects, the linear dielectric response is still visible on top of secular changes in the distribution function.

REFERENCES

1 G.R. Smith and A.N. Kaufman, Phys. Rev. Lett. 34, (1613),1975
2 A. Fukuyama et al., Phys. Rev. Lett. 38, (701),1977
3 C.F.F. Karney and A. Bers, Phys. Rev. Lett. 39, (550),1977
4 C.F.F. Karney, Phys. Fluids 21, (1584),1978 and Phys.Fluids 22,(2188)1979
5 C. Gormezano, Nucl. Fusion 21, (1047),1981
6 H. Abe et al. Phys. Rev. Lett. 53, (1153),1984
M. Ono et al. Phys. Rev. Lett. 54, (2339),1985
7 J.M.McChesney,R.A.Stern and P.M. Bellan Phys. Rev. Lett. 59, (1436),1987
8 K. Papadopoulos et al. Geophys. Res. Lett. 7, (1014),1980
9 F.Doveil Phys. Rev. Lett. 46, (532),1981
10 F.Skiff, F.Anderegg and M.Q. Tran Phys. Rev. Lett. 58, (1430),1987
11 D.F.Escande, Physics Reports 121, (167),1985
12 A.J. Lichtenberg and M.A. Lieberman, Regular and Stochastic Motion, (Springer-Verlag, New York, 1983) p.300
13 F.Skiff et al. to be published in Phys. Rev. Lett.
14 F.Skiff and F.Anderegg Phys. Rev. Lett. 59, (896),1987
15 T.Good et al. Optical diagnosis of electrostatic waves in the ion gyrofrequency range via the ion dielectric response, Contributed paper to international Workshop, Cargèse,1988
16 M.Q. Tran, P. Kohler, P.J. Paris and M.L.Sawley, Centre de Recherche en Physique des Plasmas Report LRP 205/82 (1982)
P. Kohler, R.A. Stern, B.A. Hammel, M.Q. Tran, B.M. Lamb, P.J. Paris and M.L. Sawley, Proceedings of Contributed Papers, 1984 International Conference on Plasma Physics, Lausanne, edited by M.Q. Tran and M.L. Sawley, Vol. 2, p.317
17 D.N. Hill, S. Fornaca and M.G.Wickham Rev. of Sci. Inst. 54, (309),1983
18 F.Anderegg et al. Phys. Rev. Lett. 57, (329),1986
19 R.A. Stern, D.N. Hill and N. Rynn, Phys. Lett. 93A, (127),1983
20 F.Skiff et al. Proceedings of the 1987 International Conference on Plasma Physics, Kiev, USSR, Vol.1 p.55 and Proceedings of Invited Papers (World Scientific, Singapore, 1987) Vol.1 p.441
21 J.Goree et al. Phys. Fluids, 28, (2845),1985
22 F.Anderegg et al. " An optical Carriage for LIF in Magnetised Plasma " Accepted for publication in Rev. of Sci. Inst.

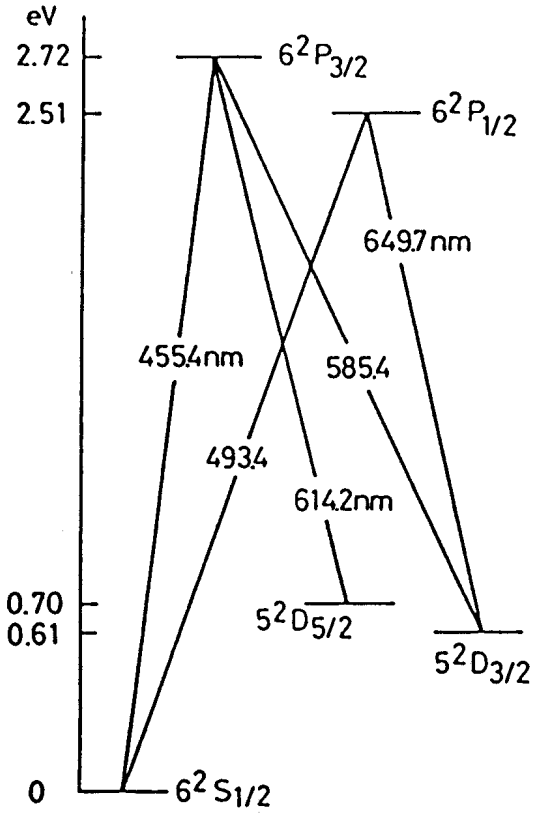

Figure 1a
Partial energy level diagram of the Barium ion

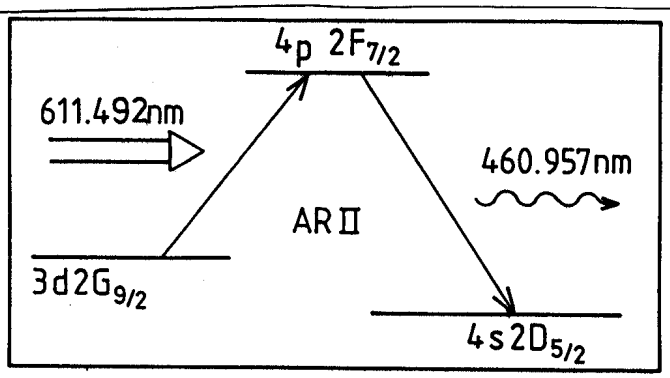

Figure 1b
Partial energy level diagram of the Argon ion

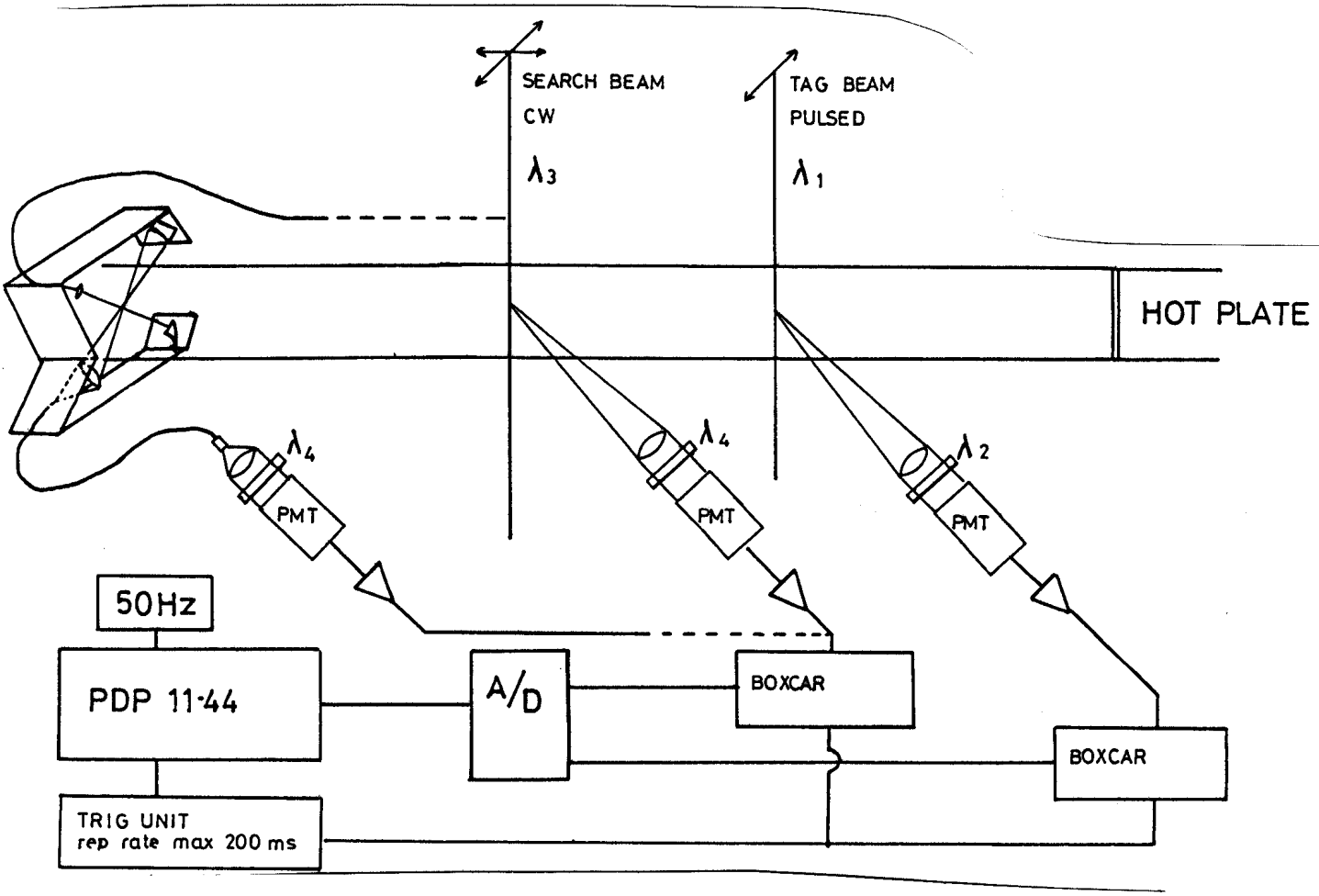

Figure 2
Representation of the optical tagging diagnostic on barium plasma. The search beam can be transported through the air or through fiber by means of an optical carriage scanable along and across the plasma column.
λ_1 = 493.4nm, λ_2 = 649.7nm, λ_3 = 585.4nm, λ_4 = 455.4nm

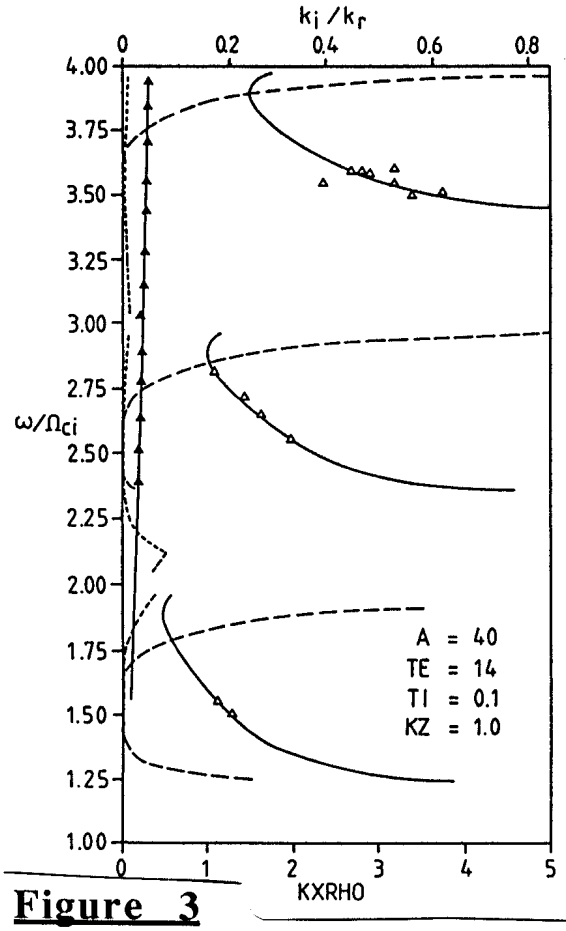

Figure 3

Linear electrostatic dispersion relation in an argon plasma. Triangles indicate experimental measurements. Dashed lines (dotted resp) indicate calculated damping for NIBW (resp EICW)

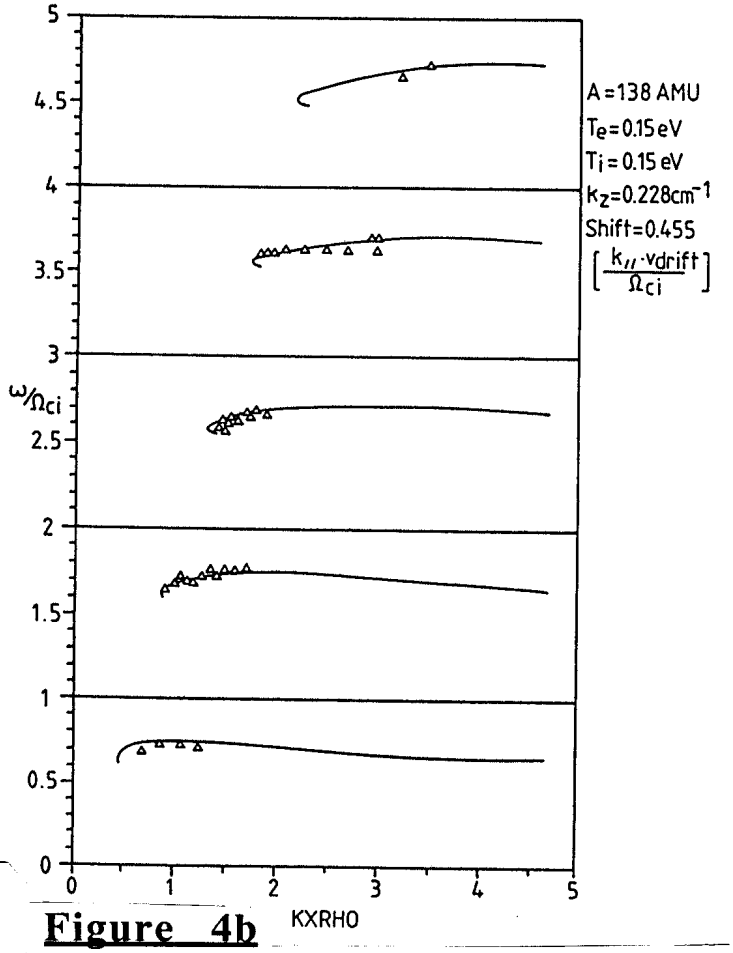

Figure 4b

Linear electrostatic dispersion relation in barium Q-plasma

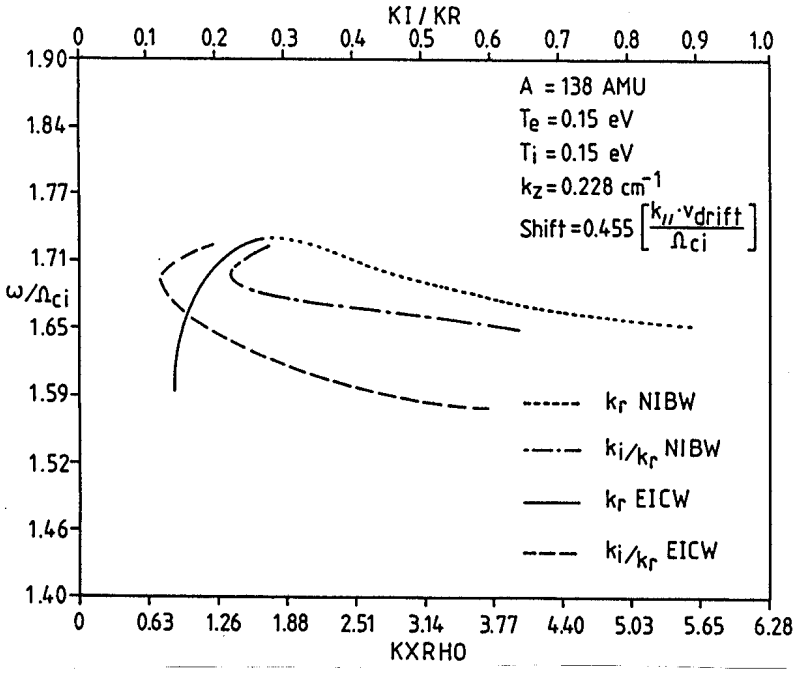

Figure 4a

Details of one harmonic of the linear electrostatic dispersion relation in barium plasma

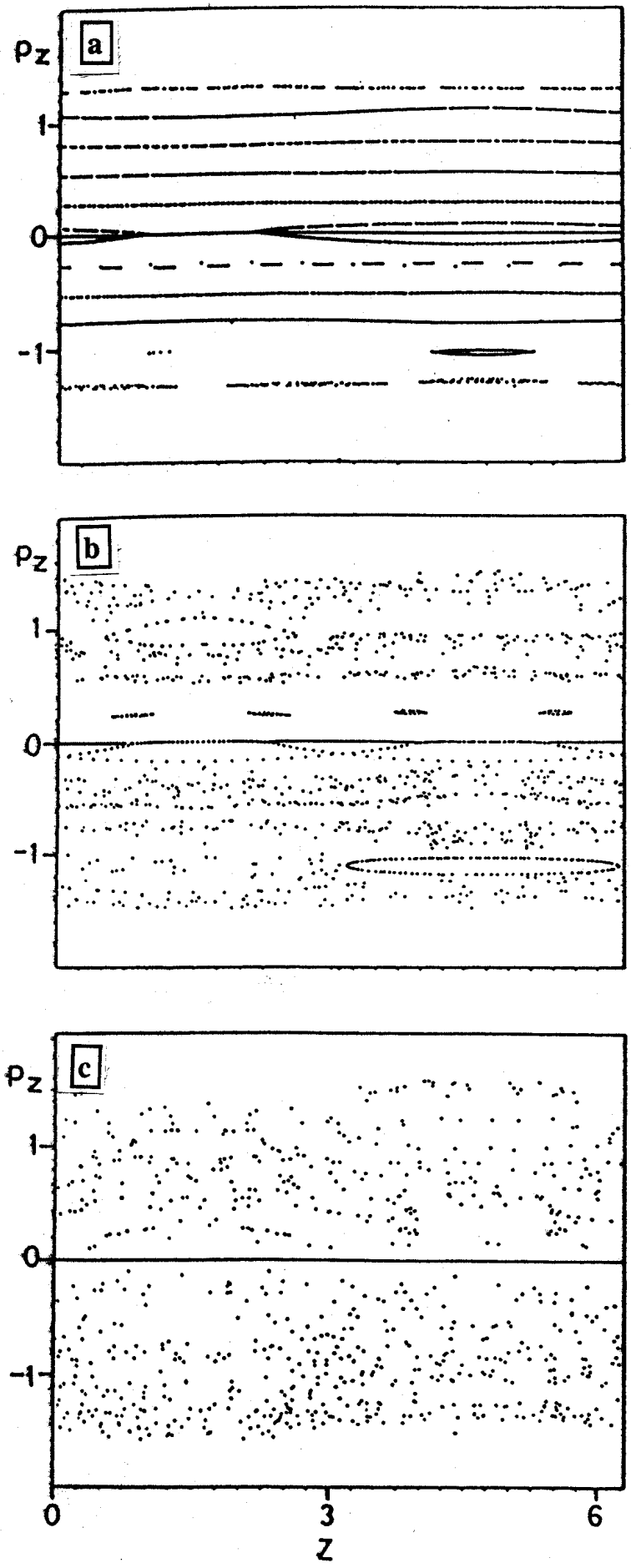

Figure 5a,b,c
Poincaré section of the phase space evolution in the p_z-z plane for a) ε=0.03, b) ε=0.16 and c) ε =0.3

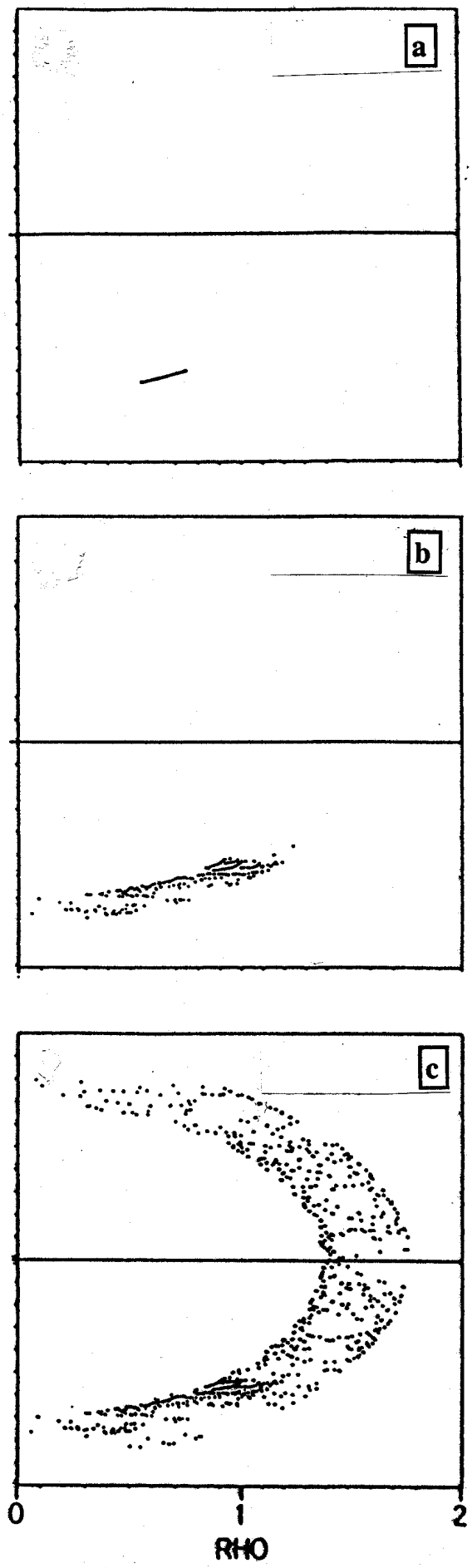

Figure 6a,b,c
Poincaré section of the phase space evolution in the p_z-ρ plane for a) ε=0.03, b) ε=0.16 and c) ε =0.3
p_z=-1 correspond to the lab. ref. frame

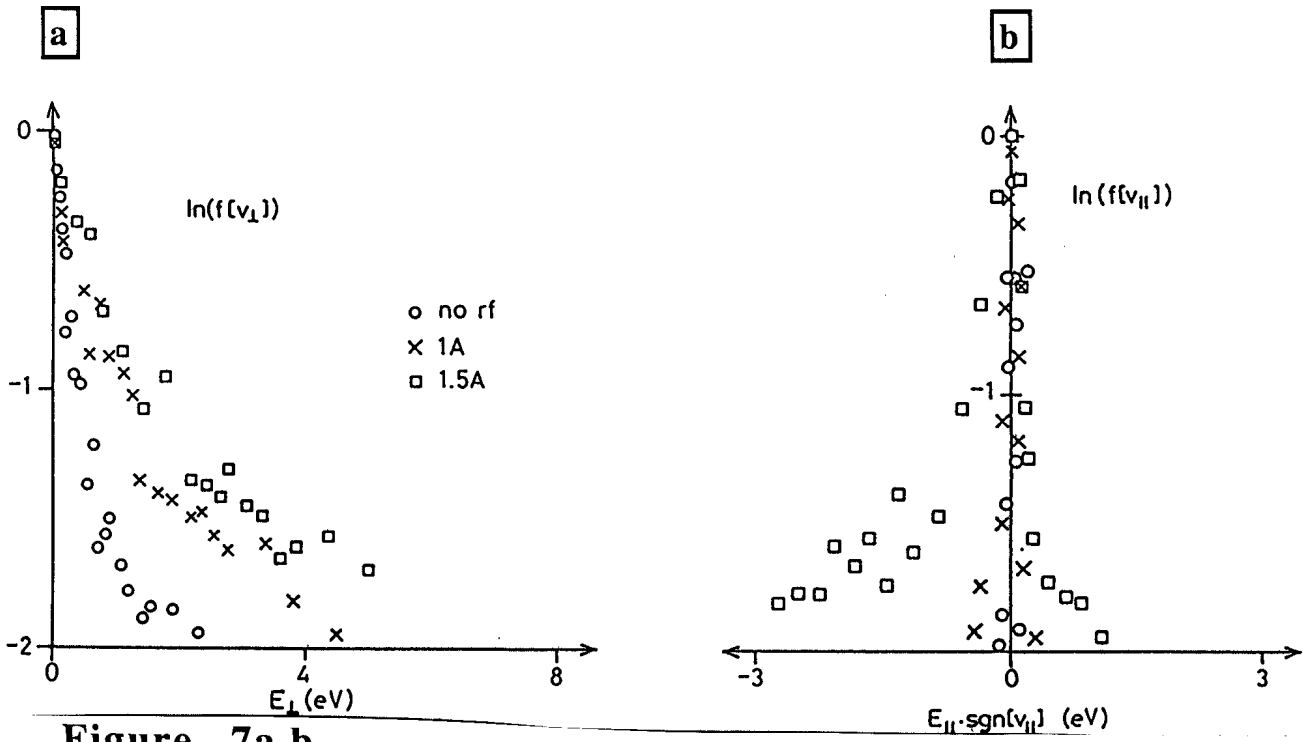

Figure 7a,b

Barium ion distribution functions in the perpendicular (a) and the parallel direction (b) as a function of wave amplitude $\varepsilon = 0$ ($I_{rf} = 0$), $\varepsilon = .2$ ($I_{rf} = 1.A$), $\varepsilon = .3$ ($I_{rf} = 1.5A$) . The wave propagates in the negative parallel direction.

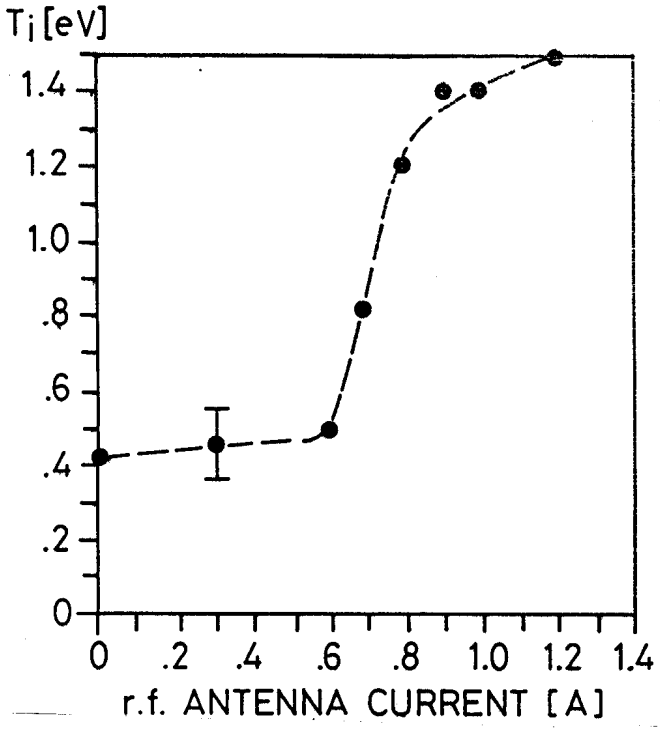

Figure 8

Argon ion temperature as a function of antenna current

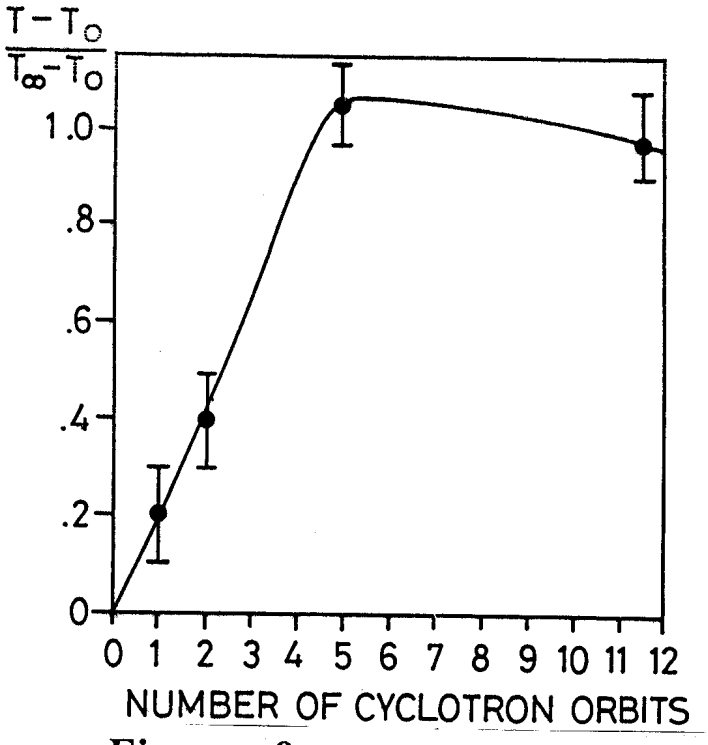

Figure 9

Time evolution of the ion temperature with a pulsed rf signal in an argon plasma

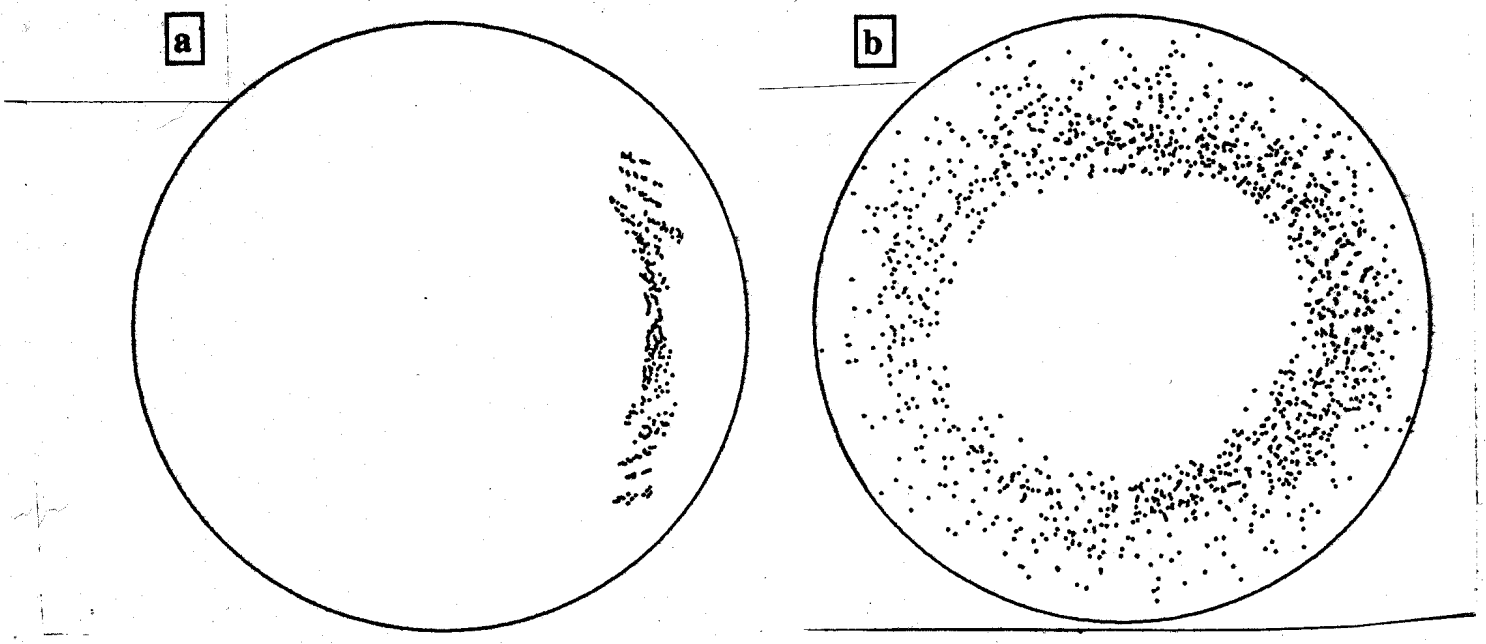

Figure 10a,b
Poincaré section in real space below (a) and above (b) the threshold. Particles have been started along a vertical chord normal to B in order to simulate the tagging experiment.

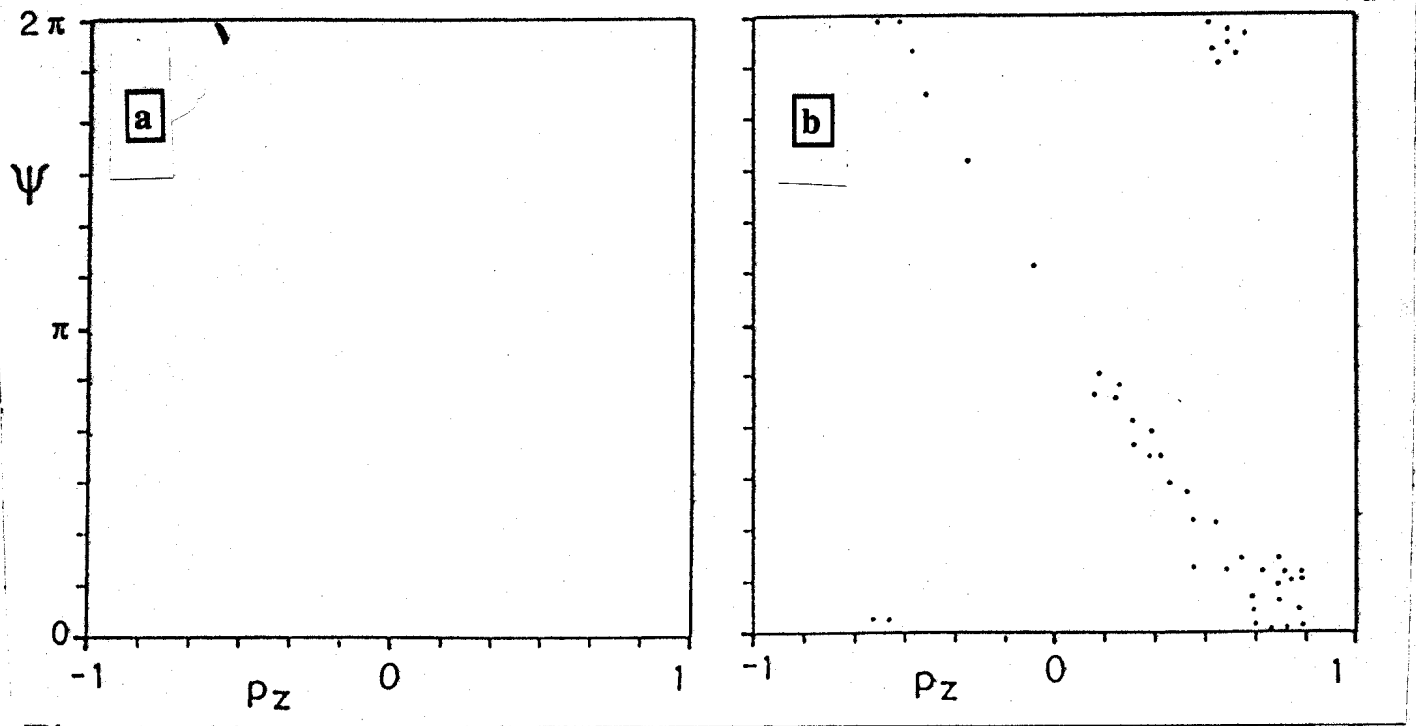

Figure 11a,b
Poincaré section for one particle in the ψ-p_z plane below (a) and above (b) the threshold . ψ is the angular position of the particle

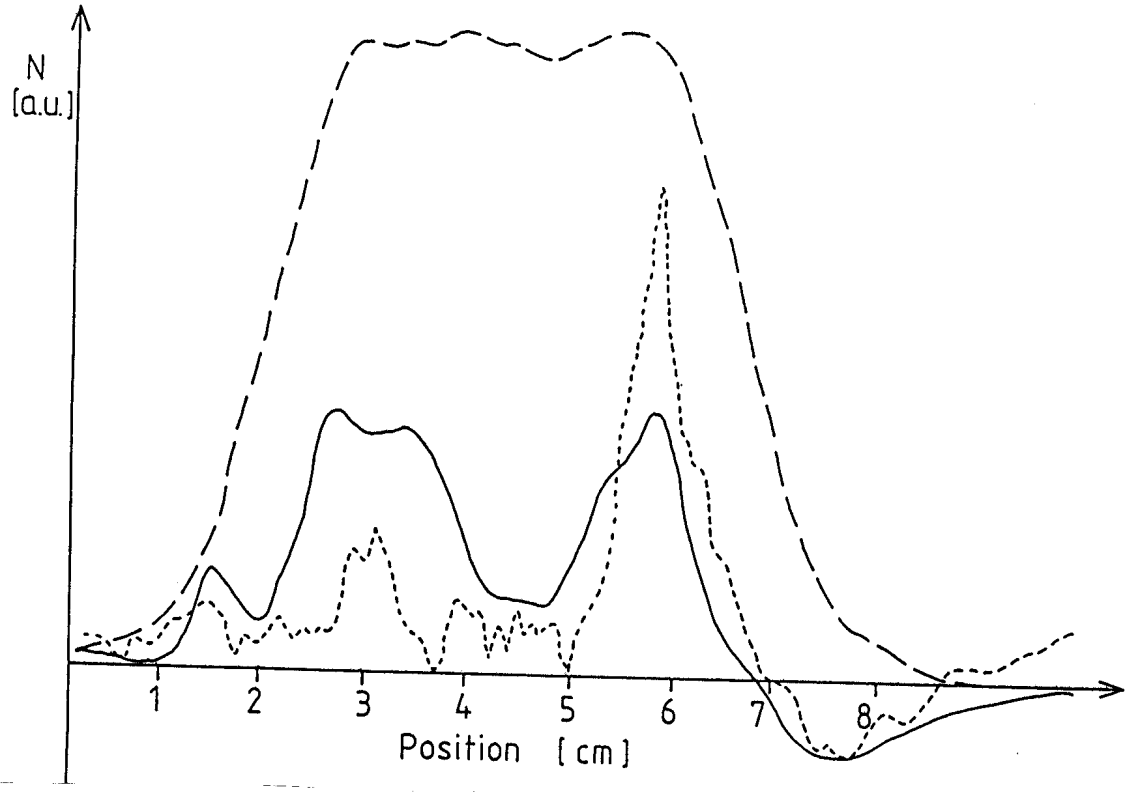

Figure 12

Density profiles on a horizontal chord. Large dash indicates electron density. Test particle density (x10) is given by small dashes (below threshold) and a solid curve (above threshold)

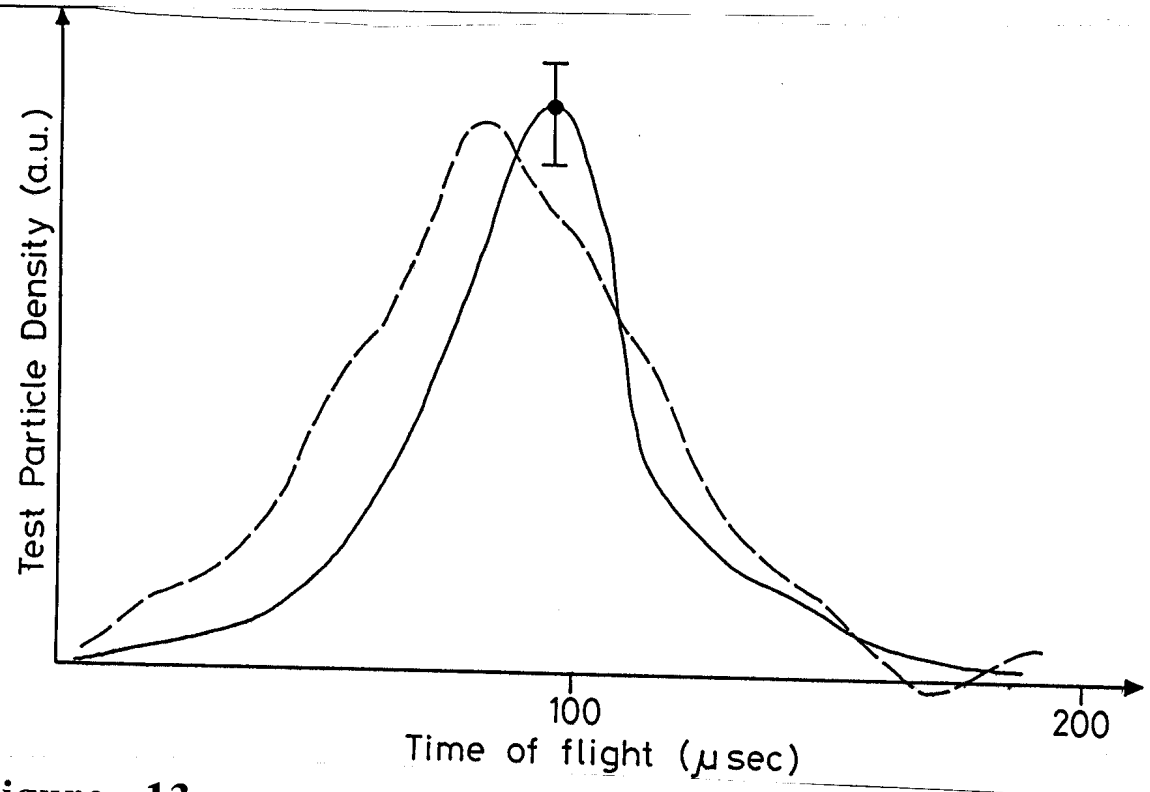

Figure 13

Time of flight spectra at R = 1.5 cm and $\psi=0$ (solide curve) $\psi=\pi$ (dashed curve)

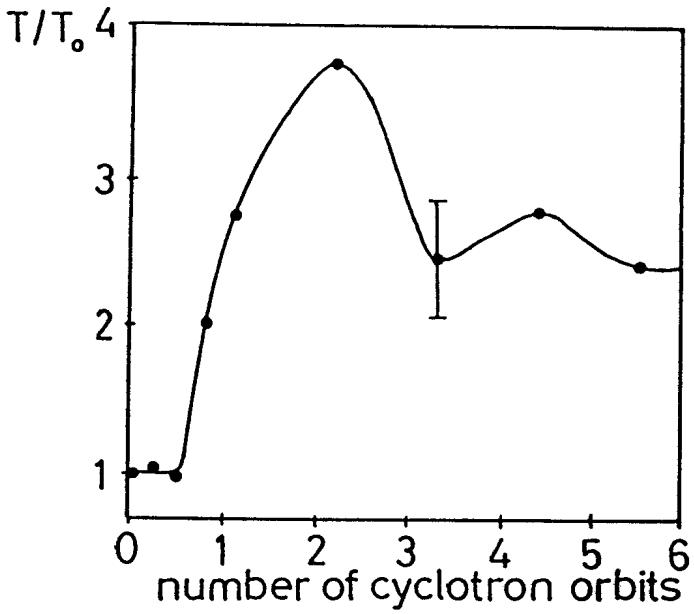

Figure 14a
Time development of barium ion temperature for pulsed rf above threshold

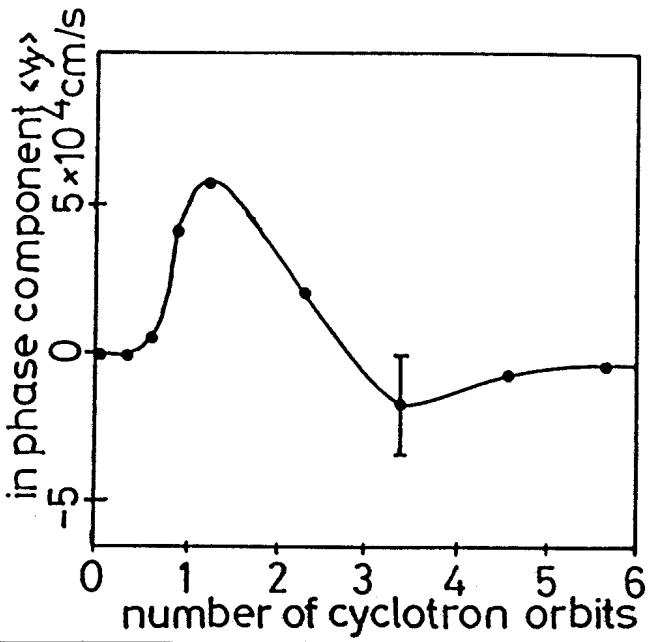

Figure 14b
Time development of the in-phase component of the dielectric velocity (amplitude of the wave)